Characterizing Amyotrophic Lateral Sclerosis progression through Extracellular Vesicles.

Author: Michell Forgione

Daily Supervisor: Suzy Varderidou

Abstract

Amyotrophic Lateral Sclerosis (ALS) is a neurodegenerative disease caused by progressive loss of motor neurons (MNs) without an available cure. Different genes had been associated with the development and progression of ALS, including Hexanuclotide repeat expansion in C9orf72, TAR DNA-binding protein 43 (TDP-43), superoxide dismutase (SOD1) and fused in sarcoma (FUS). Cell-to-cell communication can occur via extracellular vesicles (EVs) which are small vesicles released from all cell types under physiological and pathological conditions. EVs gained particular interest in the study of neurological disorders because they have the capability of spreading pathological targets to the neighboring cells. Here we used induced pluripotent stem cells (iPSCs)-derived MNs and their isolated EVs, from ALS patients, healthy control, and isogenic control lines, to measure the relative ALS-associated protein expression levels in MNs and EVs. We also treated healthy MNs with EVs derived from both ALS and healthy control MNs. First, we will demonstrate the expression of ALS-associated proteins in MNs and EVs. Then, we will show the effect of ALS-EVs on MN morphology, specifically in the number and length of dendrites, apoptosis, and mislocalization of TDP-43. Our results reveal the promising potential of iPSC-derived MNs and their EVs in the propagation of ALS-associated pathophysiology, approaching a comprehensive characterization of ALS and potential therapeutic interventions.

Introduction

Amyotrophic Lateral Sclerosis (ALS) is a neurodegenerative disorder characterized by a progressive degeneration of upper and lower motor neurons in the brain and spinal cord. It is considered the most common adult-onset disorder leading to a progressive muscle weakness. 10 % of the ALS cases have a positive family history (familial ALS), while 90% have an unknown cause (Sporadic ALS) (Lee J & Kim H., 2017; Tamaki et al., 2023). The mean survival of patients after onset is three to five years, with respiratory failure being the main cause of death (Chio et al., 2009). Recent studies have identified over 50 potential ALS-associated gene mutations, with hexanucleotide repeat expansion being the most common in C9orf72 (C9-HRE), followed by TAR DNA-binding protein 43 (TDP-43), superoxide dismutase (SOD1), and fused in sarcoma (FUS) (Grassano et al., 2022; Sproviero et al., 2018). Despite the recent growth in studies of the pathogenesis of ALS that has contributed to a better characterization of the disease, considering different biomarkers and therapeutic options (Roy et al., 2019), the development of robust biomarkers and optimization of therapeutic interventions remain to be performed.

ALS-associated genes were shown to affect multiple cellular processes, including abnormalities in RNA processing, protein homeostasis, mitochondrial function, autophagy, (McCluskey et al., 2022), and cell-to-cell communication (Cheng & Hill., 2022), which occurs through cell-to-cell contact or the release of extracellular vesicles (Pitt, Kroemer & Zitvogel., 2016). Extracellular vesicles (EVs) are small membrane-bound vesicles released by almost all cell types into the extracellular space, under both, physiological and pathological conditions (Cheng & Hill., 2022). EVs have been classified into three main categories, exosomes (20-150 nm), microvesicles (50-1000 nm), and apoptotic bodies (500-5000 nm), according to their biogenesis, size, surface protein markers, and other features. (Lee J & Kim H., 2017). Overall, EVs have an important role in cell-to-cell communication involved in the regulation of a range of biological processes (Cheng & Hill., 2022; Lee J & Kim H., 2017).

The study of EVs has become important in the field of neurodegenerative disorders. First, because of their small size can pass the Blood Brain Barrier (BBB) being detectible in different biofluids such as cerebrospinal fluid, blood, and urine. Thus, the application of EVs as a therapeutic target, non-invasive biomarker, and novel drug delivery is being actively explored (Cheng & Hill., 2022; McCluskey et al., 2022; Gagliardi et al., 2020; Hornung, Dutta & Bitan., 2020). Second, EVs contain different cargos, including lipids, nucleic acids, and proteins (McCluskey et al., 2022; Raposo & Stoorvogel., 2013), and they acquire their pathological capability depending on their cargo (Forman, Trojanowski & Lee., 2004)

EVs are important in cell-to-cell communication, therefore they can deliver their cargo to recipient cells. In this line, EVs released by affected cells can affect and elicit a phenotypic transformation in the recipient cells (Schnatz et al., 2021). Based on *in vitro* models, it was shown that exosomes mediate the propagation of Tau aggregation between cells in Alzheimer's disease (Wang et al., 2017), and accelerated the aggregation of α-synuclein in Parkinson's disease (Grey et al., 2015).These findings underscore the involvement of exosomes in the propagation of pathological protein aggregates associated with Alzheimer's and Parkinson disease's in neurodegeneration. Recent studies showed that molecular targets such as C9-HRE, FUS, and TDP-43 have been identified in ALS-derived EVs (Roy et al., 2019). In this line, Gagliardi, et al., (2020) indicated proteins with relevance for ALS in EVs, suggesting that intercellular communication via EVs responsible for the propagation of pathogenic proteins involved in the onset and progression of the disease (McAlary et al., 2020; Collins & Bowser., 2017). However, despite these findings, the direct role of ALS pathology via EVs has not been explored.

In this study, we hypothesize that a significant portion of neurotoxicity in ALS is attributed to secreted EVs from ALS-derived Motor neurons (MNs). Our research revealed expression of ALS-associated proteins in both, MNs and their EVs. Furthermore, we provide evidence of the role of EVs in inducing alterations in cellular morphology, cell death, and triggering mislocalization of TDP-43 to the cell body and neuronal branches in healthy MNs.

Materials and Methods

Western Blot Analysis

Frozen MNs and Evs were lysed by adding Laemmli sample buffer (1,25ml Tris pH 6.8 (1M), 2ml Glycerol, 5ml SDS (10%), 1,75 ml H2O) and incubated for 5 min at 95°C, followed by incubation of 30 min on ice. Then the cells were centrifuged at 13,000 RPM for 10 min at 4 ◦C. This step was omitted for EVs to avoid the potential risk of sample loss, contamination, or alteration due to their small size and sensitivity. The supernatant (corresponding to the cells) was transferred to a new tube. To determine protein concentration, BCA assay (Thermo Scientific) was performed. A range of 60 µg of protein for cells and 50 µg of protein for Evs was loaded on 12% Acrylamide gel. To denature the proteins, loading buffer (5 µl of 4x loading buffer NuPAGE, 0.5 µl b-mercaptoethanol in 20 µl of total volume of sample in lysis buffer) was added in the samples and boiled at 95°C for 5 min. Then the samples were loaded on the gels and ran at 150V for 1h. Gels were transferred and blotted onto nitrocellulose membrane (0.45 µm, Cytiva) for 1 h at 100V. For cells, membranes were blocked in 2,5% (BSA for 1 h at room temperature and incubated overnight at 4 °C with the following antibodies: Rabbit anti-TSG10 (Invitrogen, 1:1000), Rabbit anti-Calnexin (Abcam, 1:1000), Mouse anti-C9orf72 (GeneTex, 1:500), Rabbit anti-FUS (Novus, 1:1000), Rabbit anti-FUS (Sigma, 1:1000), Mouse anti-TDP-43 (Abnova, 1:400), Rabbit anti-TDP-43 (Proteintech, 1:400), Mouse anti- phospho TDP-43 (ProteinTech, 1:400), Mouse anti-β-Actin (Sigma, 1:1000), Rabbit anti-Tubb3 (BioLegend, 1:1000); diluted in blocking solution. After incubation, blots were washed 3 times in TBS-T and then incubated for 1 h with peroxidase-conjugated secondary antibodies Goat anti-Mouse (IR800, Li-COR, 1:2000; GAMPO, Alexa 700, 1:10,000) and Goat anti-Rabbit (IR800, Li-COR, 1:2000; GARPO, Alexa 800, 1:15,000) or horseradish peroxidase-conjugated secondary antibodies Goat anti-Mouse (GAMPO, 1:10,000), Goat anti-Rabbit (GARPO, 1:15,000) diluted in blocking solution. After the incubation with the secondary antibody, membranes were washed again 3 times in TBS-T and visualized by immunofluorescence using Odyssey

scanner (Li-COR) for target proteins, or chemiluminescence visualizing proteins after ECL (Pierce Chemical). Images were analyzed by quantifying the intensity measurements of protein bands using Image J Software. For Evs, the intensity measurements were quantified in Image Studio (Li-COR) and normalized to REVERT Total Protein Stain according to manufacturer instructions.

Immunostaining

Motor neurons grown on glass coverslips were fixed with 2-4% formaldehyde for 15-20 min at room temperature. Cells were permeabilized and blocked with 0.1% Triton-X-100 and blocking buffer (1,25 mL NGS, 23,75 mL PBS 1x (mix), 75 uL Triton-X-100 10%) for 1 h, and incubated in primary antibody Mouse anti-Tubb3 (Sigma,1:500), Rabbit anti-Caspase-3 (Cell Signalling, 1:500) and Rabbit anti-TDP-43 (Proteintech, 1:500) overnight at 4 ◦C or 1 h at room temperature diluted in antibody dilution buffer (0,4g BSA + 40 mL PBS 1x(mix) +120 uL Triton-X 100 10%). The next day, coverslips were washed 3 times in PBS, followed by incubation of secondary antibody: Goat anti-Mouse (Alexa Fluor 488, Invitrogen, 1:2000), Goat anti-Rabbit (Alexa Fluor 555 LifeTechno, 1:2000) diluted in antibody dilution buffer for 1,30 h at room temperature in the dark and washed 2 times in PBS. Nuclear staining was done by incubating the coverslips in DAPI (1:800) for 20 min at room temperature in the dark, followed by 2 times washing in PBS and 1 time in demi water. Coverlips were left on a tissue protected from light, cell side up for 1 h to let it dry. Stained coverslips were mounted onto glass microscope slides ($SuperFrost^{TM}$ Plus, WMR) using $FluorSave^{TM}$ Reagent (Sigma). Fluorescence was visualized using Fluorescent microscope Zeiss

Immunofluorescence Analysis

For MNs cultured in EVs, images were evaluated at 10x and 20x magnification. Random parts of the coverslips were selected to have 10 images per condition and ImageJ Software was used for the analysis. For each condition, we quantified the total number of branches and dendrite length by using skeleton plugin [Plugins; Skeleton; Skeletonize (2D/3D)]. The positive Caspase-3 Cells were counted by Analyze particle function [Analyze; Analyze Particle].

To quantify cytoplasmic TDP-43 in MNs, at least 32 MNs from images at 100x magnification were analyzed through ImageJ. DAPI was used to create a Nuclear Mask by

converting it into a binary Mask [Process; Binary Mask], removing the noise with a Gaussian Filter (radius of 3), and thresholding using the Analyze particle function to create a selection in ROI manager, this nuclear mask was used to measure the nuclear area and nuclear mean intensity of TDP-43 in the nuclei. Then, to measure the mean cytoplasmic intensity of TDP-43 in the cytoplasm, a mask containing the nucleus and the cytoplasm was created (Large Mask) by generating a threshold that segmented the cells. If cells were not well segmented we use the pencil tool to separate them. To quantify the cytoplasmic fluorescence mean Intensity, we have to calculate the cytoplasmic intensity and cytoplasmic area as described in the Supplementary Figure 1. Finally, the cytoplasmic/nuclear mean intensity ratio was calculated.

TDP-43 in the cell bodies and neuronal branches were quantified using at least 10 images per condition at 100x magnification. Analysis was done through ImageJ. A mask of Tubb3 was created to measure the fluorescence mean intensity of Tubb3, and TDP-43 in the cell body and branches of MNs. DAPI was used to count the total number of cells in each image. The mean intensity of Tubb3 and the mean intensity of TDP-43 were individually divided by the total number of cells. Subsequently, the TDP-43 mean intensity divided by cells was normalized to Tubb3 mean intensity divided by cells.

Statistics

Statistical significance between three or more values was performed by one-way ANOVA with Bonferroni's post hoc test. For experiment involving two independent variables, a two-way ANOVA with Bonferroni's post hoc test was employed. Differences between two values were determined by a two-tailed t-test, using Prism 9 (GraphPad). $P < 0.05$ was considered statistically significant. All results are presented as mean ± standard error of the mean (SEM) and in figures *$p < 0.05$, **$p < 0.01$, ***$p < 0.001$, and ****$p<0.0001$.

Results

1. **ALS-associated proteins expressed in iPSC-derived MNs from ALS patients.**

In order to elucidate the mechanisms underlying the EV transmission of ALS-associated proteins by affected MNs, iPSC-derived MNs from ALS patients having mutations in C9orf72, FUS, and TDP-43 were cultured (Fig.1A). To confirm the expression of ALS-associated proteins in these iPSC-derived MNs a western blot analysis was performed. The outcomes revealed a relative protein expression of C9orf72, FUS, TDP-43, and phospho

TDP-43 in iPSC-derived MNs from ALS patients and healthy controls (Fig.1 A-H). The protein expression of C9orf72 was tested in ALS-derived MNs carrying the mutation in C9orf72, healthy control MNs, and isogenic control MNs. Notably, no statistically significant differences in expression levels were found among the respective lines (Fig. 1 B, C). FUS exhibited elevated expression levels in isogenic control MNs, albeit without significant differences when compared to healthy control MNs (Fig.1 D, E). TDP-43 showed a slight upregulation in ALS-derived MNs carrying the respective mutation compared to healthy control MNs (Fig1. F, G). Finally, phospho TDP-43 expression was compared in TDP-43 ALS-MNs and healthy control MNs, revealing relatively higher protein expression in healthy control MNs although the differences are not significant (Fig.1 H, I). These results demonstrate the expression of ALS-associated proteins in the iPSC-derived MNs from ALS, healthy control, and isogenic control lines.

2. **ALS-associated proteins identified in extracellular vesicles.**

To determine whether EVs derived from the iPSC-derived MNs contain ALS-associated protein, EVs were isolated using ultracentrifugation (Fig. 1A), and the relative protein expression levels were assessed through western blot analysis. Western blot analysis results showed expression of TDP-43 protein in healthy control EVs and ALS-derived EVs isolated from MNs having a mutation in C9orf72, and TDP-43 (Fig. 2 A). Similarly, bands corresponding to phospho TDP-43 were observed in EVs from healthy control, as well as ALS-derived EVs from C9orf72 MNs and their isogenic control (Fig. 2B). Notably, the expression of phospho TDP-43 in TDP-43-derived EVs could not be tested (Fig. S2 A). ALS-derived EVs from MNs carrying the mutation in FUS expressed relatively high FUS protein levels, in comparison with healthy control EVs and their isogenic control (Fig.2 C, D, S2 B). However, this result is not statistically significant. These findings indicate the presence of ALS-associated proteins in EVs derived from ALS MNs despite the lack of statistical significance in the results.

3. **Healthy MNs cultured with ALS-derived EVs.**

To study if ALS-derived EVs play a role in ALS propagation, healthy MNs were treated with EVs derived from ALS-MNs carrying the mutation in C9orf72, healthy control MNs, and isogenic control MNs for 2-days. Due to the unknown EV concentration effect, we added three different concentrations to the MNs: EVs derived from 2000 MNs referred to low concentration, EVs derived from 20.000 MNs referred to medium concentration, and EVs

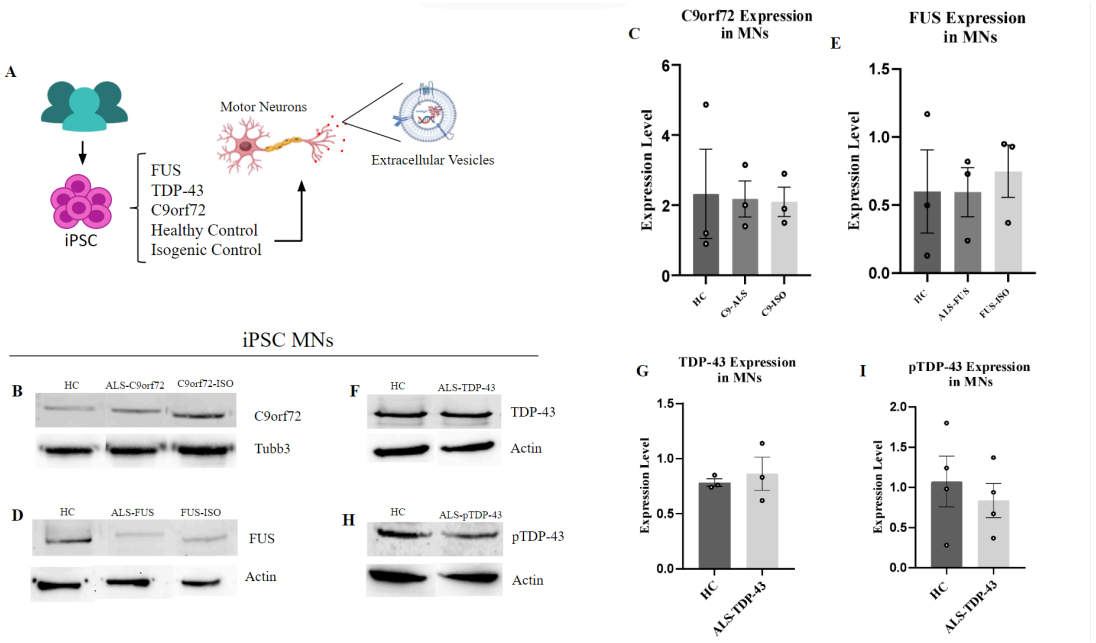

Figure 1|ALS-associated proteins expressed in ALS-derived MNs. **(A)** Experiment description. ALS-derived iPSCs carrying mutation in FUS, TDP-43 and C9orf72, along with iPSCs from healthy lines and generated isogenic control lines, were differentiated into MNs (Day 27). After the differentiation process, MNs were leve 48 hours in culture with media containing EVs, subsequently, EVs were isolated though Ultracentrofugation. (**B-I**) Western blot analysis of iPSC MNs and their respective quantification**. (B and C)** C9orf72 protein in ALS-derived MNs carrying the mutation in C9orf72, isogenic control and healthy control, normalized by Tubb3. **(D and E)** FUS protein in ALS-derived MNs carrying the mutation in FUS, isogenic control, and healthy control. **(F and G)** TDP-43 protein in ALS-derived MNs carrying the mutation in TDP-43 and healthy control. **(H and I)** Phosphorylated TDP-43 in ALS-derived MNs carrying the mutation in TDP-43 and healthy control. FUS, TDP-43 and phospho TDP-43 were normilized by Actin. Graphs are showing the quantifications of relative intensities of the Western blot analysis of three experiments per condition. Error bars indicate the mean ± SEM.

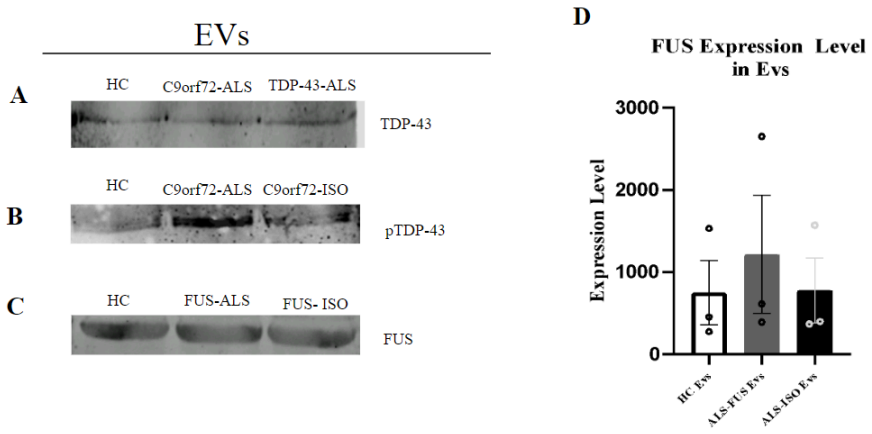

Figure 2| ALS-associated Protein expressed in EVs. **(A)** Western Blot Analysis of TDP-43 in ALS-derived EVs carrying the mutation in TDP-43, C9orf72, and a healthy control lines. **(B)** Phosphorylated TDP-43 in ALS-derived EVs carrying the mutation in C9orf72 and healthy control. **(C)** FUS in ALS-derived EVs carrying the mutation in FUS, isogenic

control, and healthy control**. (D)** Quantification of the relative intensity of FUS in ALS lines and Healthy Control. The graphs values were repeated three times. Error bars indicate the mean ± SEM.

derived from 2000.000 MNs referred to high concentration. After the culture period, MNs were fixed for subsequent immunostaining analysis.

To study the effect of EVs on healthy MNs, morphological changes, specifically alterations in the total number of neurite branches and average dendrite length, were measured. To identify the optimal condition for the analysis, images were taken at two magnifications 10x and 20x (Fig.S3, Fig.S4). Subsequently, immunostaining analysis of High Concentration (20x) (Fig.3A) revealed a significant reduction in the number of branches in MNs cultured with isogenic control EVs compared to those cultured with healthy control EVs (**P<0.01). (Fig.3C). Similarly, the number of branches in MNs cultured with ALS-EVs was relatively lower compared to healthy control-EVs MNs. The average dendrite length decreased in MNs cultured with ALS EVs, compared to healthy control EVs; however, these changes were not statistically significant (Fig. 3D).

To investigate neuron death in MNs cultured with ALS-derived EVs, we stained for Caspase-3, which is an apoptosis marker, and the number of positive Caspase-3 cells was counted. The number of positive Caspase-3 cells raised in MNs treated with ALS-Evs and their isogenic control line compared to MNs treated with healthy control-EVs. MNs showed a reduction in apoptosis when treated with healthy control-EVs, relative to healthy MNs. In contrast, MNs treated with isogenic control EVs reveal a significant increase in cell death compared to healthy MNs (Fig. 3E).

4. **TDP-43 mislocalized to the branches of healthy MNs treated with ALS-derived EVs.**

To study the effect of EVs in TDP-43 mislocalization, healthy MNs were treated with EVs derived from 2000.000 MNs carrying C9orf72 mutation, healthy control MNs, and isogenic control MNs for two days. Cells were then fixed for immunostaining analysis, and the cytoplasmic/nuclear ratio was calculated, with values indicating <1 for nuclear, 1 for equal distribution, and >1 for cytoplasmic localization. The results showed TDP-43 expression, especially in the nucleus (Fig. 4 A, B). First, we compared TDP-43 expression levels in healthy MNs and ALS-MNs revealing nuclear TDP-43 (<1), with no differences between these two conditions. Then, we compared TDP-43 expression levels in healthy MNs treated with ALS-EVs and healthy control-EVs. Notably, ALS-EV treatment showed

predominantly nuclear TDP-43 (<1), but also some equal distribution between nucleus and cytoplasm (1). In contrast, TDP-43 expression is predominantly nuclear (<1) in healthy control EV treatment despite showing slight upregulation compared to untreated conditions (Fig.4 B). These findings reveal signs of mislocalization when healthy MNs are treated with ALS-EVs.

Additionally, because we observed TDP-43 in the neurite branches we tested TDP-43 expression levels normalized to Tubb3 in ALS-MNs and healthy MNs (Fig.4 C). This result showed increased TDP-43 in ALS MNs, compared to healthy MNs. Then we compared TDP-43 expression normalized to Tubb3 in MNs treated with healthy control-EVs and ALS-EVs. TDP-43 expression levels are higher in ALS-EV treatment relative to healthy control-EVs. Notably, healthy MNs treated with ALS-EVs revealed slightly upregulated TDP-43 compared to ALS MNs and isogenic control-EVs (Fig.4 C). These findings indicate the effect of ALS-derived EVs in TDP-43 mislocalization to the neurite branches.

Discussion

We have demonstrated the expression of ALS-associated proteins in ALS-derived iPSC-MNs and their isolated EVs. Furthermore, our study reveals that healthy MNs exhibit morphological changes, apoptosis, and mislocalization of TDP-43 to the neuronal branches when cultured with EVs derived from ALS MNs. These findings support the recent reports that highlight the pathogenic role of genetic mutations in C9orf72, FUS, and TDP-43 in ALS (Prasad et al., 2019; Suk et al., 2020; Eck et al., 2021). Moreover, our results support the notion that EVs can spread neuropathological agents and modulate the phenotype of recipient cells (Krämer & Kuo, 2016).

Albeit there are no statistically significant differences observed in the level of expression of ALS-associated protein in MNs and their EVs across conditions, our findings confirm the expression of these ALS-associated proteins in healthy control and ALS MNs, and their EVs. Our results are consistent with the statement that EV cargo is related to their cell of origin (Lee & Kim, 2017), and can contribute to our understanding of EVs' capacity to deliver mutant proteins in ALS (Schanatz et al., 2021).

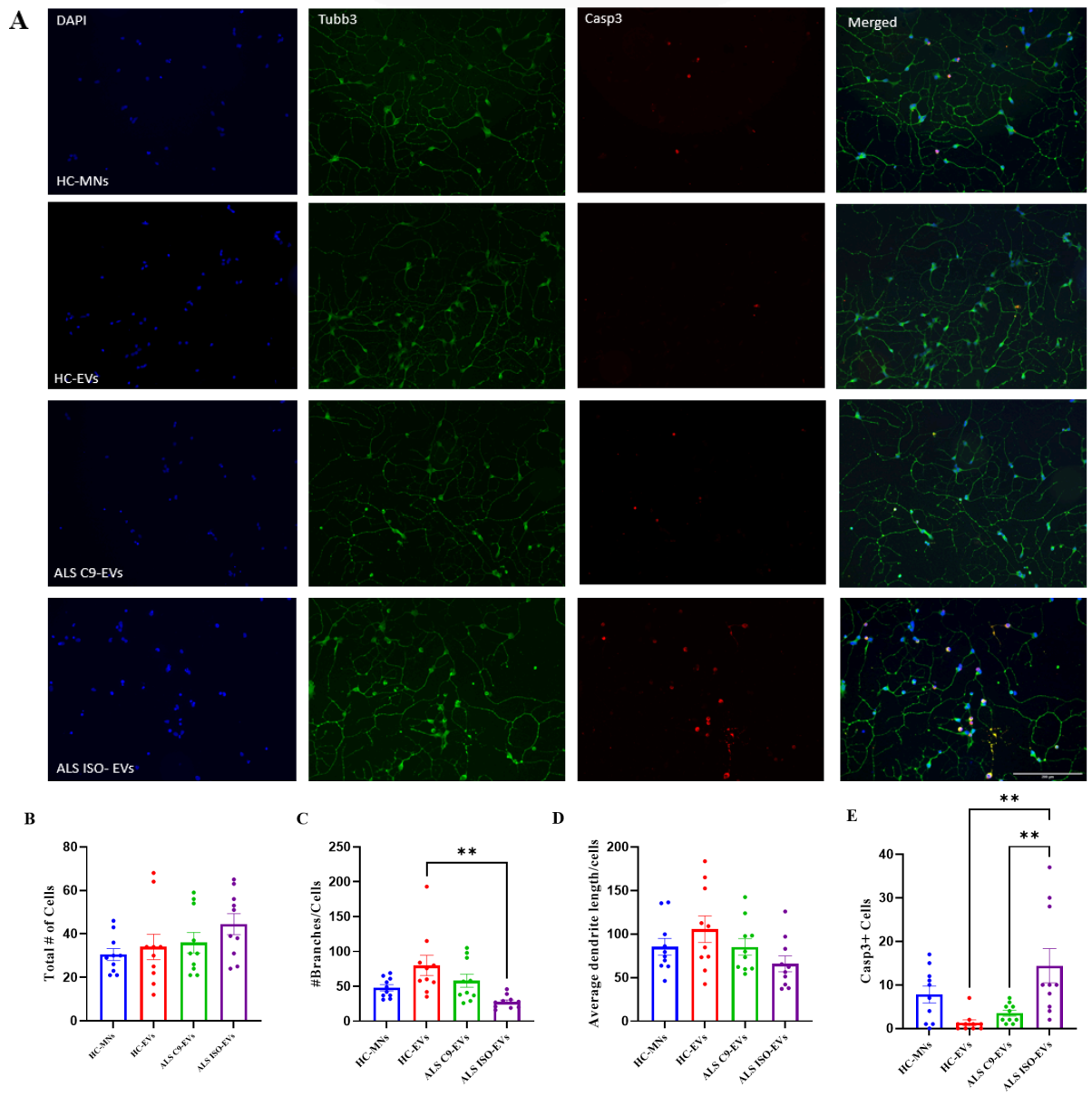

Figure 3|Healthy MNs treated with ALS-derived Evs. (A) Immunofluorescence images of MNs without EV treatment, MNs treated with healthy control EVs, C9-ALS EVs, and Isogenic Control EVs from high concentration. MNs were stained with a neuronal marker (Tubb3), an apoptosis marker (Caspase-3), and a nuclear marker (DAPI). Scale bar =100µm. **(B)** Quantification analysis of DAPI that represents the total number of cell per image. (**C**) Caspase-3-positive cells counted per image. (**D and E**) Quantification analysis of Tubb3 represented in (**D**) number of branches and (**E**) average dendrite length normalized to the number of DAPI-positive cells nuclei per image. Bar plots show mean ± SEM with individual points representing each image. A total of n=10 images per condition were used. Differences were evaluated by one-way ANOVA with Bonferroni's post hoc test. (**C and E**) P-Value = **p<0.01.

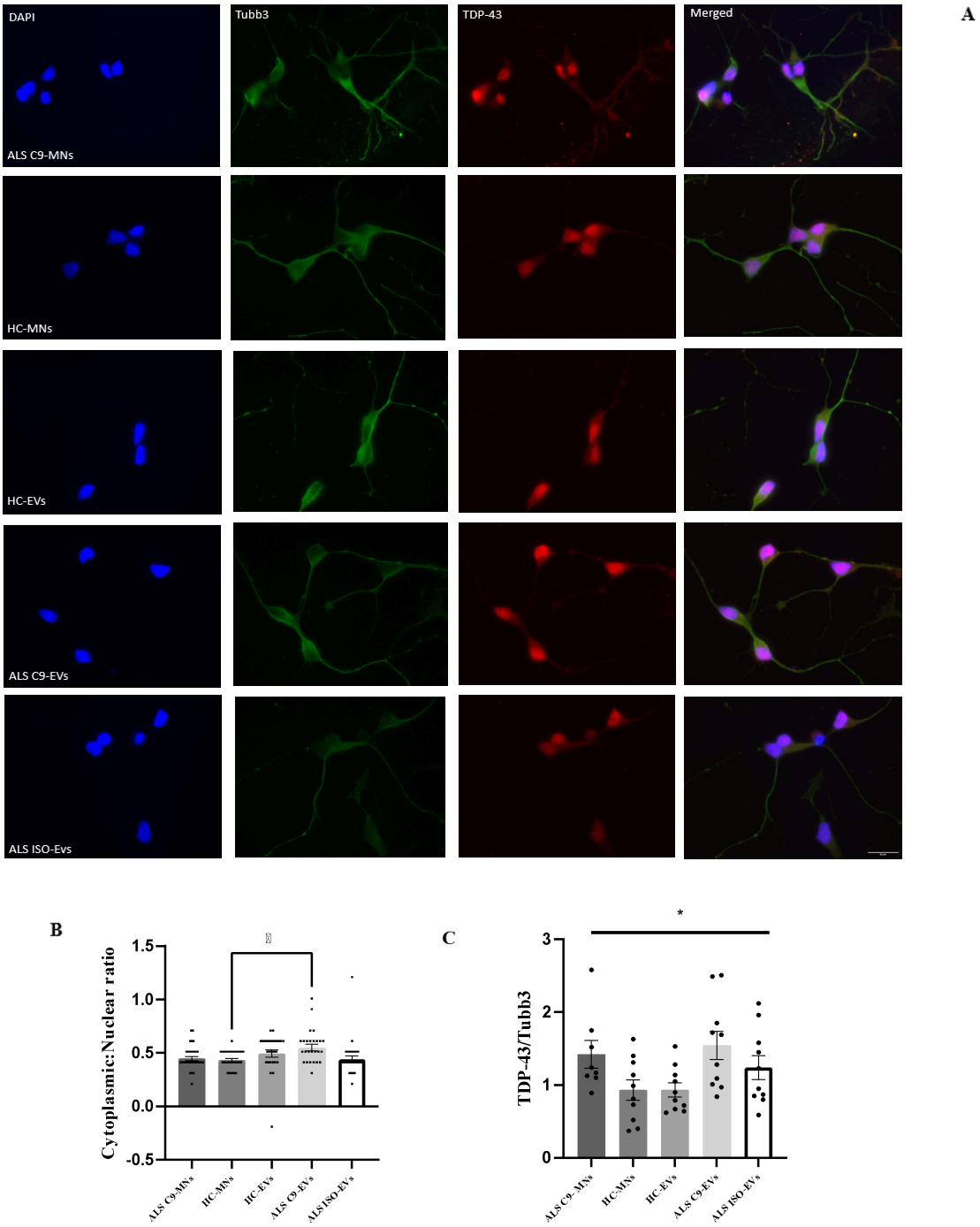

Figure 4| TDP-43 mislocalizes to MN branches in ALS. (A) Immunofluorescence images of ALS-derived MNs, healthy MNs without EV treatment, and healthy MNs treated with healthy control EVs, C9-ALS EVs, and Isogenic Control EVs. MNs were stained with a neuronal marker (Tubb3), TDP-43 antibody, and a nuclear marker (DAPI). Scale bar =20µm. **(B)** Quantification analysis of TDP-43 in the cell body and neural branches divided by the total number of cells per image (DAPI) and neuronal marker mask (Tubb3). Bar plots show mean ± SEM with individual dots representing each image analyzed (ALS C9- MNs, n: 8; HC-MNs, HC-EVs, ALS C9-Evs and ALS ISO-Evs, n: 10). **(C)** Quantification of Cytoplasmic: Nuclear ratio (>1: Nuclear; 1: Equal; <1: Cytoplasmic). Bar plots show mean ± SEM with each dot representing an individual cell body measured (ALS C9- MNs, n: 32; HC-MNs, n:28; HC-EVs, n: 27; ALS C9-Evs, n: 26; ALS ISO-Evs, n: 29). Differenced were evaluated by one-way ANOVA with Bonferroni's post hoc test. *p<0.05.

A fundamental finding in this research is the involvement of ALS-derived EVs carrying mutated C9orf72 in propagating pathological features to healthy MNs. Hexanucleotide repeat expansion in C9orf72 represents the most common genetic alteration underlying ALS pathology (Yoshitsugu et al., 2016), leading to morphological modifications in MNs, showed a significant reduction in the total length of the dendrites and the total number of dendrites branches (Huber et al., 2022). We showed that healthy MNs cultured with EVs derived from ALS-derived MNs with C9orf72 mutation and their isogenic control had a decrease in both, the total number of branches and average dendrite length compared to MNs cultured with healthy control EVs. This indicates that ALS-EVs can propagate ALS-associated pathology such as neurite loss. Remarkable, the observed increase in the number of positive Caspase-3 cells, an apoptosis marker, in MNs cultured with ALS-derived EVs, suggests that C9orf72 pathology induces dysfunction and cell death in MNs (Sellier et al., 2016, Beckers et al., 2023). These pathological features can be transmitted via EVs, validating the role of EVs in the propagation of pathogenic proteins in neurodegenerative conditions, as previously proposed (Krämer & Kuo, 2016).

A prominent hallmark of ALS is the cytoplasmic mislocalization in TDP-43, (Beckers et al., 2023; Scotter, Chen & Shaw., 2015) it is a characteristic observed in ALS patients, including patients with C9orf72 mutation (Cook et al., 2020; Beckers et al., 2023). Our outcomes, however, reveal predominant nuclear TDP-43 in ALS-derived MNs and healthy control MNs. Notably, when healthy MNs were cultured with EVs, specifically EVs derived from ALS-MNs carrying the mutation in C9orf72, TDP-43 levels were found to be similar in the nuclei and cytoplasm. While previous investigations on TDP-43 primarily focused on its cytoplasmic mislocalization in MN cell bodies (Oyston et al., 2021), recent evidence indicates that TDP-43 mislocalization plays a role in ALS through multiple pathways and is commonly observed in axons (Altman et al., 2023).). In line with this, our study detected TDP-43 expression in the neurite branches of ALS-derived MNs compared to healthy control MNs. Similarly, when we treated healthy MNs with ALS-EVs TDP-43 expression levels increased, suggesting a mislocalization of TDP-43 to the neurite branches of the cell when treated with affected EVs

There are some limitations to this study. Measuring the relative protein expression in EVs was challenging, attributed to factors such as sample characteristics, and the normalization method. Initially, we were using TSG101, an EV marker, as a housekeeping antibody; however, because immunofluorescent analysis should not cross antibodies from the

same animal species, we had to perform a stripping protocol that affected the results. Consequently, the methodology was modified to total protein quantification. Additionally, we exclusively used ultracentrifugation as the EV isolation method, future investigation may consider the incorporation of secondary separation techniques, such as polymeric precipitation, immunoaffinity, or size exclusion chromatography (Kim et al,. 2022; Varderidou & Lorenowicz., 2020) to enhance the western blot analysis results. Moreover, due to time limitations we only had isogenic control lines for C9orf72 and FUS lines, future studies should include isogenic control lines for TDP-43 as well to obtain robust comparisons. Regarding the experiment of MNs cultured with EVs, using a higher concentration of EVs could enhance the induced EV effect to explore the potential transmission of ALS pathology through EVs, also, exploring the morphological changes and TDP-43 mislocalization in healthy MNs cultures with ALS-derived MNs carrying different mutations, such as TDP-43 and FUS is recommended. Additionally, phospho TDP-43 could be considered for future measurements of healthy MNs cultured with EVs, based on their implication of ALS pathology (Altman et al., 2023). Finally, further work and replications are needed to validate the involvement of EVs in spreading ALS pathology.

In conclusion, our results provide evidence of ALS-associated protein expression in MNs and their secreted EVs. Moreover, our study establishes the EV capacity to spread these pathogenic proteins, as evidenced by alteration in morphology, cell death, and TDP-43 mislocalization to the neuronal branches of healthy MNs cultured with ALS-derived EV. These results contribute to a better understanding of the role of EVs in the propagation of ALS-related pathological and underscore their potential impact on neurodegeneration.

References

Altman et al., (2021). Axonal TDP-43 condensates drive neuromuscular junction disruption through inhibition of local synthesis of nuclear encoded mitochondrial proteins. *Nature Communications*. 12. https://doi.org/10.1038/s41467-021-27221-8

Beckers et al., (2023). A toxic gain-of-function mechanism in C9orf72 ALS impairs the autophagy-lysosome pathway in neurons. *Acta Neuropathologica Communications*, 11:151 https://doi.org/10.1186/s40478-023-01648-0

Cheng & Hill (2022) Therapeutically harnessing extracellular vesicles. *Nat Rev Drug Discov 21*, 379–399. https://doi.org/10.1038/s41573-022-00410-w

Chiò A., et al (2009). Prognostic factors in ALS: A critical review. *Amyotroph Lateral Scler. 10*(5-6):310-23. doi: 10.3109/17482960802566824.

Collins & Bowser (2017). Chapter 4 - Molecular Mechanisms of Amyotrophic Lateral Sclerosis. *Molecular and Cellular Therapies for Motor Neuron Diseases. 61*-99. doi.org/10.1016/B978-0-12-802257-3.00004-3

Cook., et al (2020). C9orf72 poly(GR) aggregation induces TDP-43 proteinopathy. S*ci Transl Med. 12*(559):eabb3774. doi: 10.1126/scitranslmed.abb3774.

Eck et al., (2021). Regulation of TDP‑43 phosphorylation in aging and disease. *GeroScie*nce. 43:1605–1614. doi: 10.1007/s11357-021-00383-5.

Forman M., Trojanowski J & Lee V (2004). Neurodegenerative diseases: a decade of discoveries paves the way for therapeutic breakthroughs. *Nat Med. 10*(10):1055-63. doi: 10.1038/nm1113.

Gagliardi D, Meneri M, Saccomanno D et al., (2019) Diagnostic and prognostic role of blood and cerebrospinal fuid and blood neuroflaments in amyotrophic lateral sclerosis: a review of the literature. *Int J Mol Sci 20*(17):4152. https://doi.org/10.3390/ijms2 0174152

Grey et al., (2015). Acceleration of α-synuclein aggregation by exosomes. *J Biol Chem*. 290(5):2969-82. doi: 10.1074/jbc.M114.585703.

Grassano M., et al (2022). Systematic evaluation of genetic mutations in ALS: A population-based study. *J. Neurol. Neurosurg. Psychiatry*. 93:1190–1193. doi: 10.1136/jnnp-2022-328931.

Hornung S., Dutta S., Bitan G (2020). CNS-derived blood exosomes as a promising source of biomarkers: opportunities and chal lenges. *Front Mol Neurosci 13*:38. doi.org/10.3389/fnmol .2020.00038

Krämer & Kui (2016). Extracellular Vesicles: Goodies for the Brain?. *Neuropsychopharmacology. 41*(1):371-2. doi: 10.1038/npp.2015.242.

Kim et al., (2022). Pathogenic Extracellular Vesicle (EV) Signaling in Amyotrophic Lateral Sclerosis (ALS). Neurotherapeutics. 19:1119–1132.

Lee J., Kim H (2017). Extracellular Vesicles in Neurodegenerative Diseases: A Double-Edged Sword. *Tissue Eng Regen Med.* 14(6):667-678. doi: 10.1007/s13770-017-0090

McCluskey G., et al (2022). Extracellular Vesicles in Amyotrophic Lateral Sclerosis. *Life (Basel). 13*(1):121. doi: 10.3390/life13010121.

McAlary et al., (2020) Amyotrophic Lateral Sclerosis: Proteins, Proteostasis, Prions, and Promises. Front. Cell. Neurosci. *Sec. Cellular Neuropathology*. 14-202.doi.org/10.3389/fncel.2020.581907

Oyston et al., (2021). Rapid in vitro quantification of TDP-43 and FUS mislocalisation for screening of gene variants implicated in frontotemporal dementia and amyotrophic lateral sclerosis. *Scientific Reports*.

Pitt, Kroemer & Zitvogel., (2016). Extracellular vesicles: masters of intercellular communication and potential clinical interventions. *J Clin Invest*. 1;126(4):1139-43. doi: 10.1172/JCI87316.

Prasad et al., (2019). Molecular Mechanisms of TDP-43 Misfolding and Pathology in Amyotrophic Lateral Sclerosis. *Front.Mol. Neurosci.,12* https://doi.org/10.3389/fnmol.2019.00025

Raposo G & Stoorvogel W (2013). Extracellular vesicles: exosomes, microvesicles and friends. *J Cell Biol.* 200:373–83. doi.org/10.1083/jcb.201211138

Roy., et al (2019). Extracellular vesicles and their diagnostic potential in amyotrophic lateral Sclerosis. *Clinica Chimica Acta.* 497:27-34. doi.org/10.1016/j.cca.2019.07.012

Schnatz et al., (2021). Extracellular Vesicles in neural cell interaction and CNS homeostasis. *FASEB Bioad*v. 3(8): 577–592. doi: 10.1096/fba.2021-00035

Scotter, Chen & Shaw (2015). TDP-43 Proteinopathy and ALS: Insights into disease mechanisms and therapeutic targets. *Neurotherapeutics.* 12(2):352-63. doi: 10.1007/s13311-015-0338-x.

Sellier et a., (2016) . Loss of C9ORF72 impairs autophagy and synergizes with polyQ Ataxin-2 to induce motor neuron dysfunction and cell . *The EMBO Journal*. 35:1276-1297https://doi.org/10.15252/embj.201593350

Sproviero D., et al (2018). Pathological Proteins Are Transported by Extracellular Vesicles of Sporadic Amyotrophic Lateral Sclerosis Patients. *Front Neurosci*.12:487. doi: 10.3389/fnins.2018.00487.

Suk, et al., (2020). The role of TDP-43 mislocalization in amyotrophic lateral sclerosis. *Neurodegeneration. 1*5:45 https://doi.org/10.1186/s13024-020-00397-1

Tamaki et al., (2023). Spina cord extract of amyotrophic lateral sclerosis spread TDP-43 pathology in cerebral organoids. *Plos genetics.* doi.org/10.1371/journal.pgen.1010606

Varderidou & Lorenowicz (2020). Mesenchymal stromal/stem cell-derived extracellular vesicles in tissue repair: challenges and opportunities. *Theranostics. 10*(13): 5979–5997.doi: 10.7150/thno.40122

Wang et al., (2017).The release and trans-synaptic transmission of Tau via exosomes.*Molecular Neurodegeneration.* 12, 5.

Yoshitsugu et al., (2017). C9orf72 and RAB7L1 regulate vesicle trafficking in amyotrophic lateral sclerosis and frontotemporal dementia. *Brain,* 140, 887–897, https://doi.org/10.1093/brain/awx024.

Supplementary Information

A $$Cytoplasmic\ Intensity = \{(Large\ Mask\ mean)x(Large\ Mask\ area)\} - \{(Nuclear\ Mask\ mean)x(Nuclear\ Maks\ area)\}$$

B $$Cytoplasmic\ area = Large\ Mask\ area - Nuclear\ Mask\ area$$

C $$Cytoplasmic\ Mean = \frac{Cytoplasmic\ Intensity}{Cytoplasmic\ area}$$

Figure S1| Calculation of Cytoplasmic Mean Intensity (A) Equation to calculate cytoplasmic Intensity. Cytoplasmic Intensity is obtained by subtracting the product of the mean intensity and area of the Nuclear Mask (Representing the nucleus) from the product of the mean intensity and area of the Large Mask (Representing the cytoplasm). **(B)** Equation to calculate cytoplasmic area. The Nuclear Mask area was subtracted from the Large Mask area. These calculations isolate and quantify intensity and area specific to the cytoplasm, excluding the nuclear area. **(C)** Cytoplasmic mean intensity equation. Cytoplasmic mean intensity is determined by dividing the cytoplasmic intensity by the cytoplasmic area.

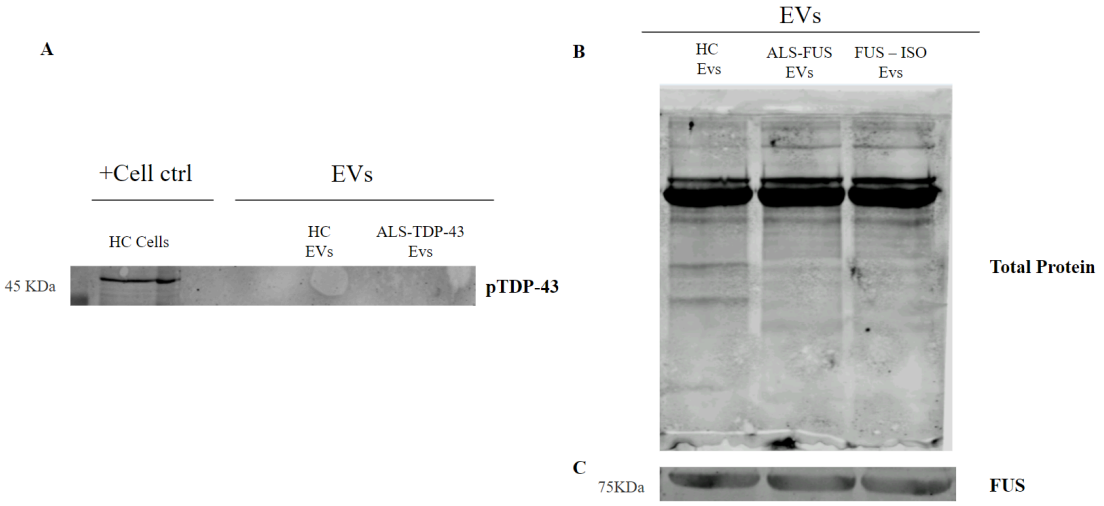

Figure S2| Phospho TDP-43 Blot and Normalization of Relative Expression of FUS in Evs. (A) Western blot analysis of TDP-43 did not show bands for phospho TDP-43 in healthy control EVs and ALS-derived EVs carrying the mutation in TDP-43. However, the positive control cells revealed the presence of phospho TDP-43 at 45KDa. **(B)** Image of nitrocellulose membrane stained with Revert Total Protein stain. **(B)** Western Blot analysis of FUS expression in Healthy control EVs and ALS-derived EVs, including Isogenic control, showing bands at 75KDa. Quantification of the Signal intensity of FUS was normalized by the signal intensity of the respective line in the total protein stain.

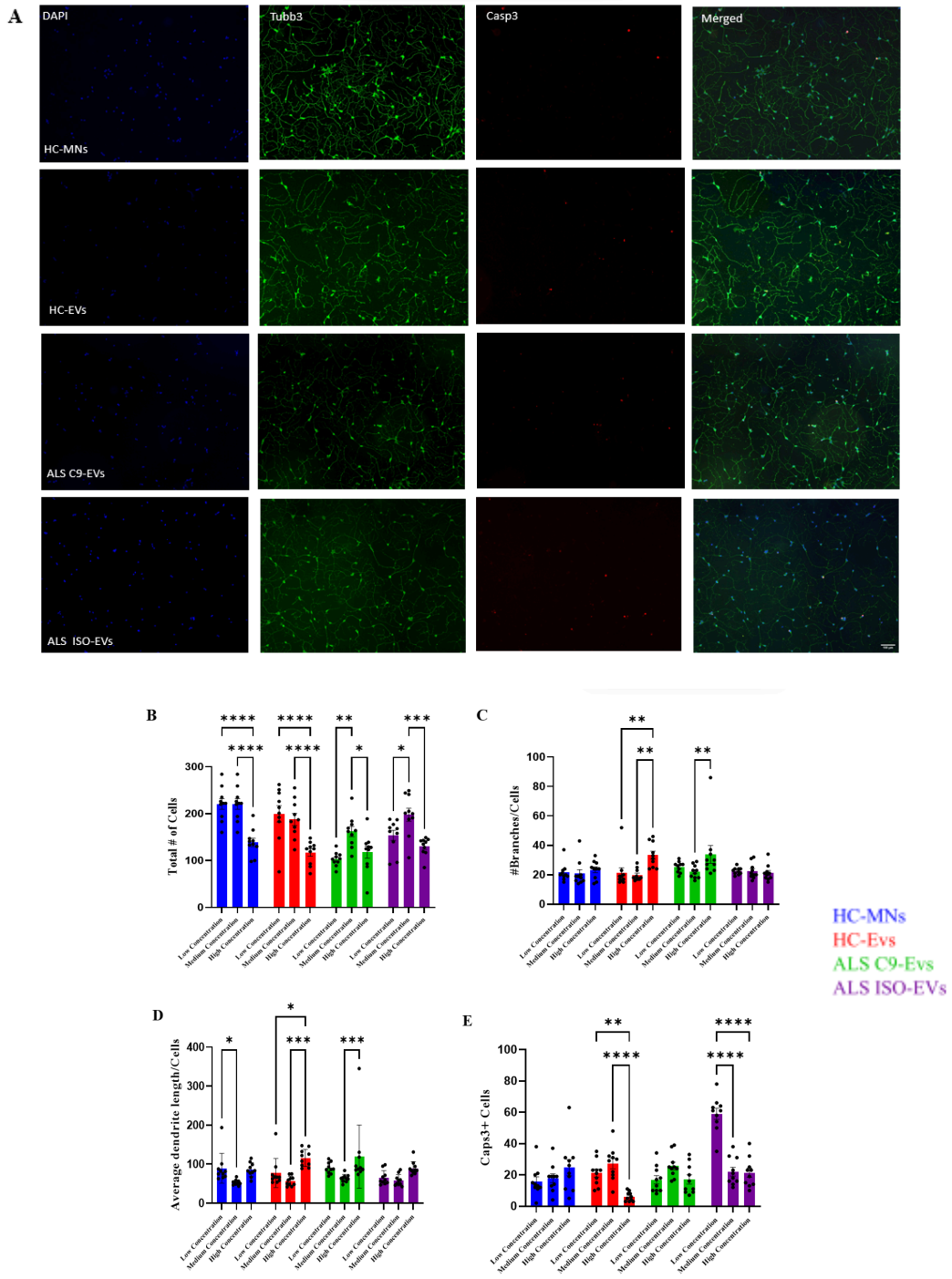

Figure S3| Immunoblotting analysis of images evaluated at 10x magnification. (A) Immunofluorescence images of MNs without EV treatment, MNs treated with healthy control EVs, C9-ALS EVs and Isogenic Control EVs from high Concentration. MNs were stained with a neuronal marker (Tubb3), an apoptosis marker (Caspase-3) and a nuclear marker (DAPI). Scale bar =200µm. **(B)** Quantification analysis of DAPI that represents total number of cell per concentration level (**C**) Caspase-3-positive cells counted per image in each concentration level. (**D and E**) Quantification analysis of Tubb3 represented in (**D**) number of branches and (**E**) average dendrite length normalized to number of DAPI-positive cells nuclei per image in each concentration level. Bar plots show mean ± SEM with individual points representing images per condition. A total of n=10 Images per condition were used. Differences were evaluated by two-way ANOVA with Bonferroni's post hoc test. (**B-E**) P-value= *<0.05, ** <0.01, ***<0.001, ****<0.0001.

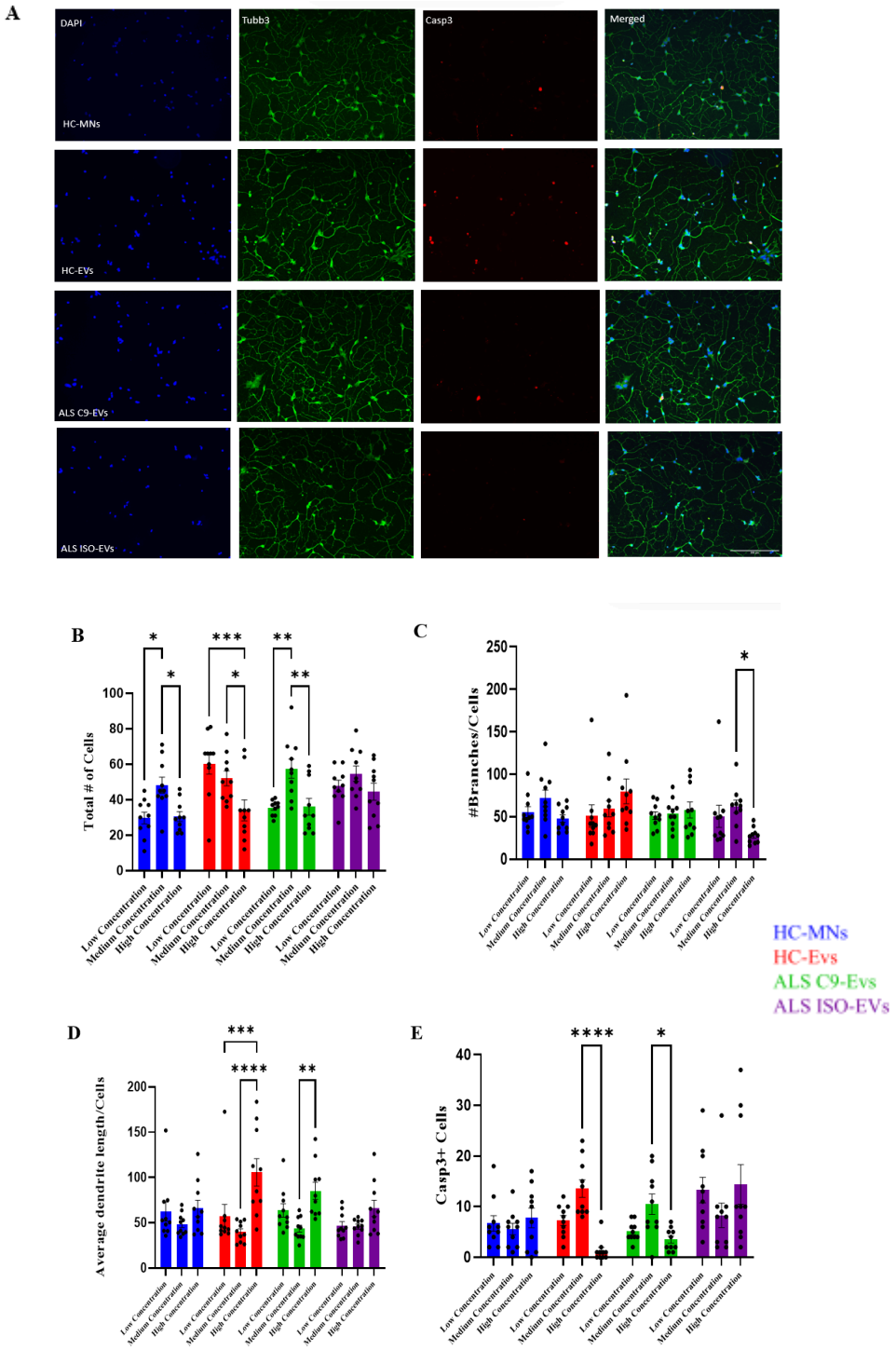

Figure S4| Immunoblotting analysis of images evaluated at 20x magnification. (A) Immunofluorescence images of MNs without EV treatment, MNs treated with healthy control EVs, C9-ALS EVs and Isogenic Control EVs from medium concentration. MNs were stained with a neuronal marker (Tubb3), an apoptosis marker (Caspase-3) and a nuclear marker (DAPI). Scale bar =100µm. **(B)** Quantification analysis of DAPI that represent total number of cell per concentration level (**C**) Caspase-3-positive cells counted per image in each concentration level. (**D and E**) Quantification analysis of Tubb3 represented in (**D**) number of branches and (**E**) average dendrite length normalized to number of DAPI-positive cells nuclei per image in each concentration level. Bar plots show mean ± SEM with individual points representing images per condition. A total of n=10 Images per condition were used. Differences were evaluated by two-way ANOVA with Bonferroni's post hoc test. (**B-E**) P-value= *<0.05, ** <0.01, ***<0.001, ****<0.0001.